Robust Optimal Control of a Neutral-Atom Quantum Processor

Nathan Wagner,[1,2] Jeffery Larson,[1] and Matthew Otten[2]
[1)]*Argonne National Laboratory, 9700 S. Cass Avenue, Lemont, 60439, IL, USA*
[2)]*Department of Physics, University of Wisconsin-Madison, 1150 University Avenue, Madison, WI, USA*

(Dated: Friday 2nd August, 2024)

We propose an implementation of a CZ gate for a neutral-atom quantum computer which is robust against noise. Although high-accuracy gates have been designed for neutral-atom computers, the design of gates resistant against noise found in experiments has not been widely explored in literature. To design a robust gate special considerations must be taken into account, such as correct parameters to be robust against, an efficient metric which may differentiate against robust and non-robust gates, and an efficient solver. The gate proposed is shown to maintain an average gate fidelity of > 0.92, an improvement from 0.65 using a non-robust gate, under pertubations in commonly noisy parameters.

INTRODUCTION

As technology is increasingly dependent on understanding the quantum world, the ability to simulate complicated quantum dynamics becomes more important. This are notoriously hard to simulate classically, but can be done by leveraging the unique properties of quantum physics on a quantum computer. In this way, quantum simulation and computing holds promise to provide a significant speedup to intractable problems in computing. However, these computers are currently prone to noise, making noise mitigation incredibly important.

In this study we propose an implementation of a logical gate on a neutral-atom quantum computer that remains accurate in the presence of noise in the parameters. Gates on quantum computers are very sensitive to noise, and traditionally implementations of gates have been determined without taking into account experimental inaccuracy. This noise is shown to have a non-negligible effect on the efficacy of the gate, meaning the accuracy of implementations found using non-robust objectives may be significantly lowered under noisy conditions found in experiment. Optimal control using a metric robust against noise requires special considerations, such as the determination of correct parameters to be robust against, a metric which is able to differentiate between robust and non-robust gates, and the design of an efficient robust optimizer.

METHODS

In a neutral-atom quantum computer, qubits are encoded in an array of alkali atoms trapped in an optical lattice [1]. Alkali atoms are used because of their single valence electron, which may be manipulated freely while keeping the filled shells stable. This means we do not have to worry about multi-electron effects without having to deal with light atoms such as hydrogen. For our computer we use cesium, however rubidium has also been employed for similar purposes.

The structure of the array is created using an optical lattice. By shining lasers blue-detuned from an atomic transition, an effective energy gradient is created. This motivates the atoms to rest in locations where the intensity of the light is minimized. By shining the lasers in a grid, we are able to get the atoms to rest in a lattice.

Gates are implemented by addressing the atoms with lasers detuned from their atomic frequency. The shape of the intensity and detuning of the laser, which we refer to as the pulse shape, is important in ensuring that the correct final state is achieved from any initial state.

We are able to store quantum data in the lattice by encoding the data in energy levels of each atom. A unit of quantum data is referred to as a qubit, and may assume a 0 or a 1. However, the unique properties of quantum systems allow us to store combinations of 0s and 1s in a single qubit, or connect different qubits in a manner known as entanglement. Entanglement is one of the most important functions of a quantum computer, but it is highly sensitive to noise.

In a neutral-atom quantum computer, entanglement is achieved using Rydberg blockage. By exciting one atom to a high-energy Rydberg state, strong dipole-dipole interactions are induced between the Rydberg atom and neighboring atoms. This shifts the energy levels of the neighboring atoms, meaning that addressing a nearby atom with the same laser will not excite it to the Rydberg state, as the frequency of the laser will be wrong. By addressing an atom with a laser which only shifts the $|1\rangle$ state to a Rydberg state, we are able to impart a relative phase on the $|00\rangle, |01\rangle$ and $|11\rangle$ states.

Specifically, the gate we wish to implement is known as a controlled Z gate, or a CZ gate. These, along with CNOT gates, are the most common entangling gates employed in quantum computing. In many implementations of CZ gates on neutral-atom processors, extra logic gates are included before or after the CZ gate to correct the phase induced by the gate. These gates are known as Z gates, may introduced additional noise not found in the CZ gate itself. Therefore, we focused on the implementation of a CZ gate without corrective Z gates.

The full evolution of the system is performed under the Lindblad master equation

$$\frac{d\rho}{dt} = -i[\rho, \hat{H}] + \sum_i \left(\hat{L}_i \rho \hat{L}_i^\dagger - \frac{1}{2}\{\rho, \hat{L}_i^\dagger \hat{L}_i\} \right) \tag{1}$$

which is the most general evolution of a quantum system which preserves the trace of the density matrix. Given a pure input state ρ_{in} and an desired, pure output state ρ_{out}, the gate fidelity of a unitary gate $\hat{U}$ is defined as

$$F = \text{Tr}(\rho_{\text{out}} \hat{U} \rho_{\text{in}} \hat{U}^\dagger) \tag{2}$$

The metric then used is the average gate fidelity, or the average accuracy of the gate acting on all input states. To determine

the effect of the pulse shape on the robustness of a solution, we compare the robustness of two different pulses. One uses the parameters and pulse shape in [2], which we call the qLDPC gate. The other is the adiabatic rapid passage pulse in [3], which is referred to as the ARP gate.

The parameters used for Rydberg blockage are found on Gate 1 of [2], which uses a Rydberg blockage strength of $415.0\text{MHz}/2\pi$ corresponding to a lattice spacing of 1.7μm and the Rydberg state $|50s_{\frac{1}{2}}\rangle$. These parameters were used for both gates for consistency, although the original ARP gate in [3] is optimized under a different Rydberg blockage. The Rydberg state was also modelled as having a lifetime of $\tau_R = 60.4\text{ns}$. This is modelled by Lindblam terms $\hat{L} = \sqrt{\frac{b_s}{\tau_R}}|s\rangle\langle r|$, where b_s denotes the branching ratio to the state s. We use $b_s = \frac{1}{16}$ for the $|0\rangle$ and $|1\rangle$ states, and $b_s = \frac{7}{8}$ to a fully decoherent state $|d\rangle$. This leads to a theoretical bound on the gate error of $\varepsilon_{\min} = \frac{2}{V\tau_R} = 1.27\cdot 10^{-5}$, and a theoretical bound on the fidelity of $F_{\max} = 0.999987$.

To obtain robust optima, rather than minimizing the error itself we minimize the worst-case error obtained by perturbing the parameters around a central point

$$\min_{\vec{x}} \max_{\vec{u}\in B(\vec{x})} \varepsilon(\vec{u}) \tag{3}$$

where $B(\vec{x})$ is a neighborhood of $\vec{x}$. We call this a robust optimum, as it is more robust in the context of noisy signals. As the vector $\vec{x}$ represents a set of parameters in parameter space, it is called the center parameters.

In the context of experimental error, we assume that in the worst case all parameters may be perturbed independently of each other to a certain maximum error. Therefore the neighborhood under the L^∞ norm is used

$$B(\vec{x}) = \left\{ \vec{u} \middle| \max\left(\left|\frac{u_1 - x_1}{\delta B_1}\right|, \left|\frac{u_2 - x_2}{\delta B_2}\right|, \ldots \left|\frac{u_n - x_n}{\delta B_n}\right| \right) \leq 1 \right\} \tag{4}$$

where δB_i are maximum errors corresponding to each parameter, which we call the box widths.

Two different methods of finding the robust optimum were used. One we denote Box; because we are optimizing over a box in parameter space surrounding the center point, we can assume that the maximum of the objective is attained at one of the far corners. We then use a simplex method, with the objective being the maximum of the error at each corner of the box along with the error at the center parameters

$$\varepsilon_{\text{box}}(\vec{x}) = \max(\{\varepsilon(x_1 \pm \delta B_1, x_2 \pm \delta B_2, \ldots x_n \pm \delta B_n)\}, \varepsilon(\vec{x})) \tag{5}$$

We also use a manifold sampling algorithm presented in [4], which we denote the Manifold method. This algorithm approximates the set $B(\vec{x})$ as several selected points, which are updated throughout the run. Points are chosen which generally give the maximal error for center parameters

The box widths for both the qLDPC and ARP runs are found in tables I and II. These were selected based on experimental data found in [2] and [3], along with considerations for parameters that are generally noisy and stable in experiment. As the magnitude and shape of the detuning tends to be more prone to error than the intensity of the laser percentagewise, we include two metrics. One metric, which we call Small, employs smaller errors in pulse intensity and duration relative to errors in detuning. For example, the parameters Δ_0, a, f are perturbed relatively more compared to the parameters Ω_0, T, τ, as the former significantly control the magnitude and shape of the detuning. The other, which is named Big, includes relatively large errors in all parameters.

	$\delta\Omega_0/2\pi$	δT	$\delta\Delta_0/2\pi$	δa	δf	$\delta\tau$
Small	±0.1MHz	±2ns	±0.5MHz	±0.25	±0.5MHz	±2ns
Big	±0.5MHz	±10ns	±0.5MHz	±0.25	±0.5MHz	±10ns

TABLE I. Box widths for the Small and Big objectives for the qLDPC gate.

	$\delta\Omega_0/2\pi$	δT	$\delta\Delta_0/2\pi$	$\delta\Delta_{\text{amp}}/2\pi$	$\delta\tau$
Small	±0.1MHz	±2ns	±0.5MHz	±0.5MHz	±2ns
Big	±0.5MHz	±10ns	±0.5MHz	±0.5MHz	±10ns

TABLE II. Box widths for the Small and Big objectives for the ARP pulse.

	Non-Robust	S. Box	B. Box	S. Manifold	B. Manifold
Non-Robust	0.99978	0.983	0.9936	0.988	0.973
Small Objective	0.654	0.926	0.924	0.928	0.828
Big Objective	0.575	0.838	0.858	0.862	0.686

TABLE III. Fidelities of the optima found for the non-robust optimizer and four different robust optimizers for the qLDPC gate. The robust optimizers begun at the non-robust optimum, and the non-robust optimizer started at the parameters for Gate 1 in [2].

Simulations were performed using a JAX wrapper for QuTIP [5]. This provided us with a means of autodifferentiation with respect to input parameters, which greatly improved the efficiency of optimizers. The optimization itself was performed using a Python wrapper for NLOpt [6]. Derivative-based optimization was performed using SLSQP, and derivative-free optimization used the Subplex method.

In all cases used here, the fidelity can ultimately be written as a function of many expectation operators, which may be evaluated in parallel. Certain robust objectives such as Box further lend itself to parallel computing, as the number of sampled inputs grows exponentially with the number of parameters, leading to serial implementations of this function being incredibly slow. However, the autodifferentiation software used was not suited for flexible parallelization of the many different objectives required.

A scheme using MPI was implemented which is able to efficiently parallelize both non-robust and robust calculation of the objective. This was done by sharding the calculation of the expectation operators, which is the most computationally intensive process in calculating the objective, in addition to sharding the calculation of the many points used in the Box objective. The calculation is parallelized such that each job corresponded to one evaluation of the expectation operators of

	Non-Robust	S. Box	B. Box	S. Manifold	B. Manifold
Non-Robust	0.9990	0.9985	0.983	0.9945	0.976
Small Objective	0.810	0.813	0.806	0.908	0.897
Big Objective	0.670	0.674	0.762	0.854	0.869

TABLE IV. Fidelities of the optima found for the non-robust optimizer and four different robust optimizers for the ARP gate. The robust optimizers begun at the non-robust optimum, and the non-robust optimizer started at the parameters for [3].

a time-evolved state. This allows for flexible implementations of different metrics in a single framework while minimizing the overhead.

RESULTS

Usually, an additional corrective phase gate is included at the beginning or end of a CZ gate. This may lead to extraneous errors in practice. We found that it was possible to implement the CZ gate without corrective pulses in both the qLDPC and ARP implementations. The minimum error for the non-robust metric was found to be $\varepsilon = 2.23 \cdot 10^{-4} = 17.55\varepsilon_{\text{min}}$ in the qLDPC implementation and $\varepsilon = 1.03 \cdot 10^{-3} = 81.33\varepsilon_{\text{min}}$ for the ARP implementation.

Results for the optimization of the qLDPC and ARP gates are found in tables III and IV respectively. In both cases, robustness was found to not be guaranteed by using an optimizer which does not account for it. For example, the non-robust optima in the qLDPC implementation had a fidelity of 0.654 under the Small objective, and the non-robust ARP parameters had a fidelity of 0.810 under the same objective. In contrast, parameters for both gates were found with robust fidelities of 0.928 and 0.908 respectively under the Small objective.

The fidelities obtained for the qLDPC gate were consistently found to be higher in the Small objective than the fidelities of the ARP gate, while the fidelities in the Big objective were observed to be similar. The difference between the maximal robust fidelity in the Small objective between the two implementations was $F_{\text{qldpc}} - F_{\text{arp}} = 0.02$, while the difference of the maximal fidelities found in the Big objective was $F_{\text{arp}} - F_{\text{qldpc}} = 0.007$. It is additionally important to note that the ARP gate had less parameters to perturb against.

Parameters determined for each optimum are found in tables **??** and **??** for the qLDPC gate and the ARP gate respectively. Contour plots of the neighborhood of the solution found are shown in Fig. 1. While research in the literature has focused against robustness against pertubations in the maximum intensity and detuning of the laser, it is shown that pertubations in shape parameters must also be taken into account.

Graphs displaying the evolution of the maximally entangled Bell state $|\Phi_+\rangle = \frac{1}{\sqrt{2}}(|00\rangle + |11\rangle)$ and the state $|11\rangle$ are found in Figs. 2 and 3 for the non-robust gate and the Small Manifold gate respectively. Ideally, the state $|\Phi_+\rangle$ should end up in the state $|\Phi_-\rangle = \frac{1}{\sqrt{2}}(|00\rangle - |11\rangle)$ and the state $|11\rangle$ should return back to $|11\rangle$ by the end of the evolution. Interestingly, there are qualitative differences between the evolution of these

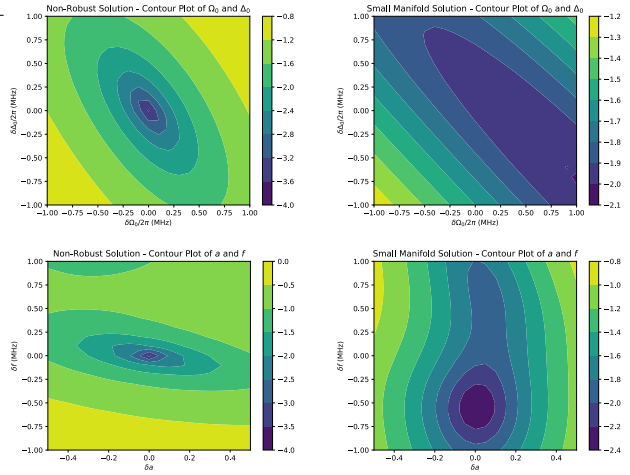

FIG. 1. Contour plots of the non-robust and Small Manifold with the qLDPC implementation. The logarithm of the error $\log_{10}(\varepsilon)$ against both pertubations in Ω_0 and Δ_0 and pertubations in a and f.

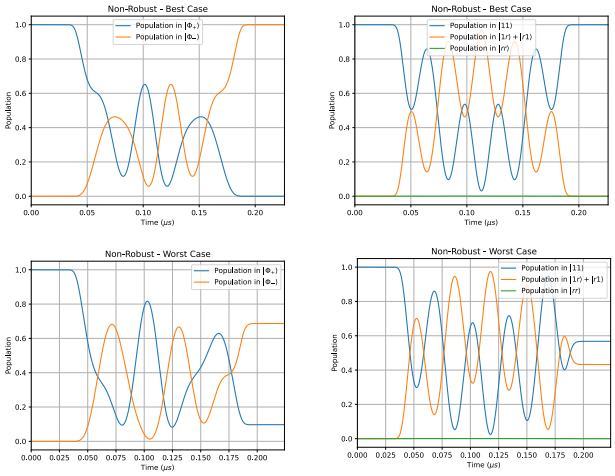

FIG. 2. Evolution of the Bell state $|\Phi_+\rangle$ and the state $|11\rangle$ under the non-robust gate using the qLDPC implementation.

two states between robust and non-robust gates, which will be a subject of future research.

DISCUSSION

As the robustness of a pulse was observed to be dependent on its shape, we plan on investigating reasoning behind why certain pulses are more robust than others in future research. Specifically, we will attempt to perform robust optimization over a wider set of pulse shapes and noisy conditions. Errors extraneous to the error in parameters, such as crosstalk or a finite atom temperature, will also be addressed in greater detail.

Our work has focused on one specific implementation of a CZ gate. Namely, the gate we propose uses a single-photon process to excite the $|1\rangle$ state to a Rydberg state. Other imple-

	$\Omega_0/2\pi$(MHz)	T(ns)	$\Delta_0/2\pi$(MHz)	a	f(MHz)	τ(ns)
Non-Robust	20.36	226.1	-14.10	7.89	4.29	1.91
Small Box	17.06	310.0	-23.44	6.04	4.36	3.00
Big Box	19.32	242.4	-24.32	6.06	4.54	1.03
Small Manifold	40.18	176.2	-26.50	7.00	10.39	1.95
Big Manifold	23.39	225.4	-11.18	6.06	6.70	1.92

TABLE V. Optimal parameters determined for the qLDPC gate.

	$\Omega_0/2\pi$(MHz)	T(ns)	$\Delta_0/2\pi$(MHz)	$\Delta_{\text{amp}}/2\pi$(MHz)	τ(ns)
Non-Robust	79.94	353.6	1.41	36.97	129.5
Small Box	79.94	352.1	1.41	36.30	129.5
Big Box	80.08	308.1	1.48	75.58	128.8
Small Manifold	88.31	234.1	2.14	76.40	134.4
Big Manifold	88.52	223.1	2.22	70.49	202.5

TABLE VI. Optimal parameters determined for the ARP pulse.

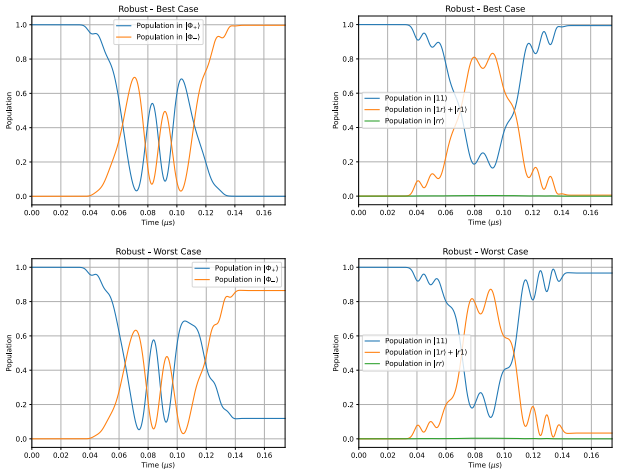

FIG. 3. Evolution of the Bell state $|\Phi_+\rangle$ and the state $|11\rangle$ under the Small Manifold gate using the qLDPC implementation.

mentations, such as the usage of a double-photon process [3] or Förester resonance [7]. These have been proposed to offer improvements on robust fidelity in certain situations.

Additionally, gates have been proposed for a neutral-atom quantum computer which entangle more than 2 qubits. We plan on investigating the feasibility of a robust implementation of these gates, along with more general entangling gates for 2 qubits, in future research.

CONCLUSION

We have shown that noise in the parameters is a nontrivial consideration for gate design. In particular, certain gates which may have high fidelity are less stable to experimental noise compared to others. We show a dependence of the robustness of a gate and the shape of the pulse, and study the properties of two different gates under experimental noise.

Additionally, parameters of a CZ gate have been proposed which are robust against error in two different implementations. In both cases robust gates maintain fidelities of > 0.9 in the presence of noise. This motivates a continued study of optimal control in the context of quantum information and the development of scalable quantum technology.

REFERENCES

[1] T. M. Graham et al. "Multi-qubit entanglement and algorithms on a neutral-atom quantum computer". In: *Nature* 604.7906 (Apr. 2022), pp. 457–462. ISSN: 1476-4687. DOI: 10.1038/s41586-022-04603-6. URL: http://dx.doi.org/10.1038/s41586-022-04603-6.

[2] C. Poole et al. *Architecture for fast implementation of qLDPC codes with optimized Rydberg gates*. 2024. arXiv: 2404.18809 [quant-ph]. URL: https://arxiv.org/abs/2404.18809.

[3] M. Saffman et al. "Symmetric Rydberg controlled- <mml:math xmlns:mml="http://www.w3.org/1998/Math/MathML"><mml:mi>Z</mml:mi></mml gates with adiabatic pulses". In: *Physical Review A* 101.6 (June 2020). ISSN: 2469-9934. DOI: 10.1103/physreva.101.062309. URL: http://dx.doi.org/10.1103/PhysRevA.101.062309.

[4] Jeffrey Larson, Matt Menickelly, and Stefan M. Wild. "Derivative-free optimization methods". In: *Acta Numerica* 28 (2019), pp. 287–404. DOI: 10.1017/S0962492919000060.

[5] James Bradbury et al. *JAX: composable transformations of Python+NumPy programs*. Version 0.3.13. 2018. URL: http://github.com/google/jax.

[6] Steven G. Johnson. *The NLopt nonlinear-optimization package*. https://github.com/stevengj/nlopt. 2007.

[7] Shuai Liu et al. *Optimized nonadiabatic holonomic quantum computation based on Förster resonance in Rydberg atoms*. 2021. arXiv: 2107.14486 [quant-ph]. URL: https://arxiv.org/abs/2107.14486.